Check for updates

Soft electrothermal actuator array for surface morphing application

Ryan Nam, Ji Eun Lee, Michael Jakubinek, Behnam Ashrafi, and
Hani E. Naguib*

Electrothermal actuators (ETAs) have been the focus of continuous R&D in targeting soft actuator applications. This article explores both the fabrication and design characteristics of a poly(dimethylsiloxane) (PDMS) elastomer—carbon nanotube buckypaper layered composite in the dual cantilever bending arrangement. Actuation characterization tests demonstrate the relationship between actuator geometries, boundary conditions, and heating rate to the maximum bending deflection. SEM observations on the cross sections of the ETAs fabricated with different conductive layers display the variations in thickness, and the effects of localized heating zones are discussed. By comparing different fabrication methods, improvements to the actuation features through ETA design modification were reported, and the possibility to greatly increase the actuation was displayed. The potential of ETAs as surface morphing actuators is demonstrated in concept through fabrication of a single sheet array consisting of multiple ETAs with the ETA segments individually and simultaneously activating to create hill-like features.

Impact statement

Exploring the fabrication of novel soft robotic actuators shows great promise in creating devices that are lightweight, flexible, and multifunctional. These actuators can provide a unique alternative to conventional mechanical solutions. For example, as lightweight and low-profile surface actuators where conventional mechanical actuators are too bulky. This article discusses an investigation of the bending deformation of various designs of electrothermal actuators and the various factors that influence the actuation performance such as geometry, electrical conductivity, and actuator fabrication methods. To better understand the behavior, several characterization tests and various fabrication methods are demonstrated. The aim is to investigate and understand the fundamental factors that influence the deformation of electrothermal actuators and develop a shape conformable array of actuators for shape-morphing applications. The overall performance of the developed actuators shows great promise for improving soft robotics systems.

Introduction

Soft robotic actuators as alternatives for conventional mechanical systems have been the focus of an extensive amount of research as the demand for miniaturization and optimization increases.[1–3] Compared to well-established mechanical systems with electric motors, actuators based on soft responsive materials can provide benefits such as greater flexibility, lower manufacturing cost, higher load-to-weight ratio, reduced size and weight, and versatility in external stimuli for actuation.[4–7] Incorporating a combination of these traits opens the possibility for usage in applications ranging from morphing structures for aircrafts[8,9] to soft robotic grippers.[10–12] In terms of readily available and accessible activation methods, electroactive polymers (EAPs) are one of the most investigated areas of

development. EAPs are most notable for their considerable induced strain produced when stimulated by an external electric field[13,14] and include material types such as ionic polymer-metal composites, dielectric elastomers, and conductive polymers.[15,16] In addition to these, there exists a group of composites called electrothermal actuators (ETAs), notably distinct from the types previously mentioned as ETAs can operate in an electrolyte-free environment under low driving voltages.[17]

The primary mechanism for ETA activation is an increase in temperature resulting in thermal expansion of the conductive composite. The heating to initiate this process is typically achieved through passing an electric current through a conductive layer.[18–20] ETA composites are typically created as a flexible

Ryan Nam, Toronto Smart Materials and Structures, Mechanical and Industrial Engineering, University of Toronto, Toronto, ON, Canada
Ji Eun Lee, Toronto Smart Materials and Structures, Mechanical and Industrial Engineering, University of Toronto, Toronto, ON, Canada
Michael Jakubinek, Division of Emerging Technologies, National Research Council Canada, Ottawa, ON, Canada
Behnam Ashrafi, Aerospace Research Centre, National Research Council Canada, Montreal, QC, Canada
Hani E. Naguib, Toronto Smart Materials and Structures, Mechanical and Industrial Engineering, University of Toronto, Toronto, ON, Canada; naguib@mie.utoronto.ca
*Corresponding author
doi:10.1557/s43577-022-00474-4

bilayer of a high coefficient of thermal expansion (CTE) polymer and a conductive film. Similar to the thermal expansion of a bimetallic strip, the heating will cause more expansion in the comparatively greater CTE polymer side and bend it toward the lower CTE side. ETAs, unlike other electrothermally driven smart materials such as shape-memory polymers with conductive fillers, have the advantages of a wider variety of materials, reversible shape change, and continuous range of bending deformation because they are not constrained by a transition temperature.[21,22] Researchers have designed grippers by taking advantage of this bending and have demonstrated bending deformations greater than 220° curvature in a period of less than 8 s.[23] Further developments in the actuator design,[24] bilayer materials properties,[25] and operating constraints[26] have been made.

An essential component of ETA performance is the preparation and composition of the conductive layer. In general, carbon nanotubes (CNTs) have commonly been utilized as a highly conductive nanofiller for advanced polymer composites.[27–29] There has been an increased interest in CNT-based composites for multifunctional applications because CNTs display great mechanical strength, low density, high flexibility, and excellent electrical conductivity.[30,31] However, a frequent limitation to CNT incorporation is the uniformity in dispersion. Due to their large surface area resulting from their high-aspect ratio, the van der Waals interactions between individual nanotubes leads to considerable amounts of nanofiller agglomeration.[32] Inconsistencies in dispersion produced from agglomeration can manifest in unexpected mechanical, thermal, and electrical properties that can be detrimental to actuator performance and lifetime.[33] In a study by Ahn et al., heterogenous ETAs were fabricated by sonicating a solution of CNTs mixed with Ag nanowires and spray coating a fabric substrate to create the conductive layer.[34] Martinez-Rubi et al. demonstrated the fabrication of high CNT content composite sheets through a one-step vacuum filtration process with tailorable mechanical and electrical properties.[35]

This study investigates and optimizes the design and control of poly(dimethylsiloxane) (PDMS)/CNT composites through various fabrication methods and characterizations. This includes the actuation trends between actuator dimensions, the distance between the fixed constraints, and heating rate to the observed bending deflection in the fixed beam configuration. In comparison to studies that use thin polymer composite films of ≤65 μm,[36] ETA composites in this article will be fabricated thicker for more significant bending deformation. This will also demonstrate the feasibility of ETAs as a durable morphing surface with controlled morphing features. To progress toward this design, the fabricated individual actuators will be operated in a both-ends-fixed arrangement, unlike the more commonly displayed cantilever for mechanical grippers,[37,38] or the free standing configuration to illustrate lateral movement.[34,39] Analysis on fabrication methods will compare the CNT conductive layer of ETA prepared through
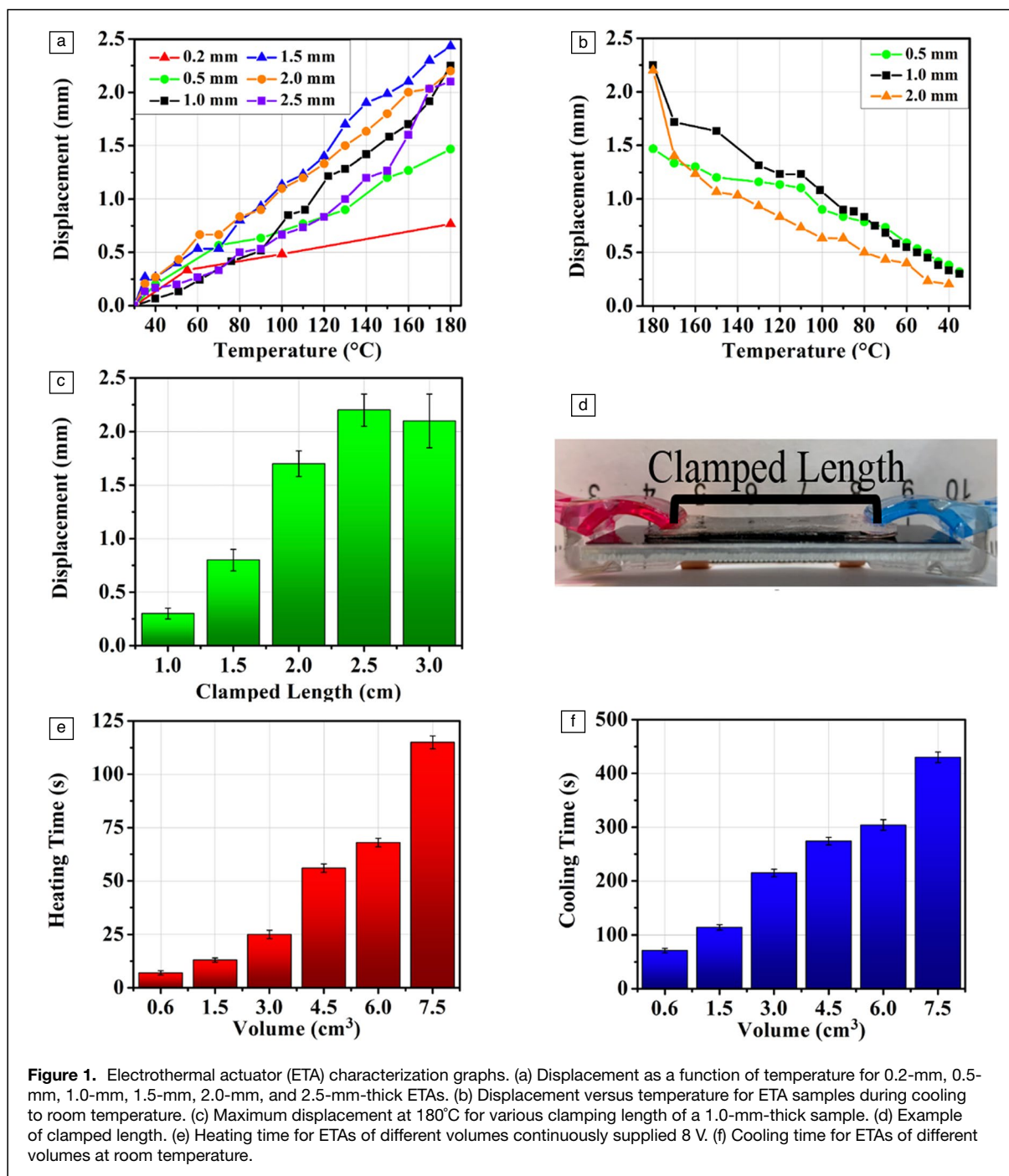
solution casting versus recovered by filtration method. It has been noted by Hajiesmaili et al. that by designing a thickness gradient in the conductive layer, the shape morphing of the elastomer can be controlled by the spatial variations when activated.[40] The uniformity of shape morphing will be investigated as it is affected by the conductive layer thickness due to the fluctuations in resistance and stiffness. Utilizing the results of these observations, a shape conformable ETA array capable of individual and simultaneous shape morphing will be fabricated and demonstrated.

Results and discussion

Characteristics of electrothermal actuators

The development of the electrothermal actuators (ETAs) began with the investigation of its actuation mechanisms. Soft polymer-based ETAs are fabricated by bonding an elastomer to a conductive filler layer chosen with highly dissimilar coefficients of thermal expansion (CTE), these being PDMS and CNT, respectively, in this study. Because the elastomeric and conductive layers of the bilayer actuator have significantly different values of CTE, the composite will bend toward the layer with the lower CTE. This behavior is comparable to the heating of a bimetallic strip, where two metals are bonded and when fixed on one end and heated, will bend toward one side. Bending is favored toward the lower CTE layer, but factors such as elasticity and layer thickness will affect the degree of deformation. The composite was found have a CTE of 361 ± 13 μm/m°C when measured from room temperature to 200°C using a thermomechanical analyzer in our previous related study.[39] The other influential materials properties were the thermal diffusivity of 0.133 ± 0.013 mm²/s, and the specific heat capacity of 3.02 ± 0.15 J/g°C at 200°C. The mechanical properties of the PDMS/CNT bilayer were characterized revealing an elastic modulus of 4.57 ± 2.03 MPa, and an ultimate yield strength of 1.03 ± 0.19 MPa. The resistance of the conductive layer before the addition of PDMS was 0.12 ± 0.02 Ω. Once the actuator was fully assembled, the resistance across five tested samples increased to 11.7 ± 6.3 Ω when measured using a multimeter.

Actuator thickness, the distance between the constraints, and the heating duration are several of the factors expected to influence the total bending deflection. These factors were characterized and plotted through a series of tests (**Figure 1**). To maintain consistency within the tests, the ETA samples were constructed with the same dimensions, a width and length of 1 cm and 3 cm, respectively. The thermal decomposition of PDMS and reduction in mechanical properties begins at temperatures greater than 200°C.[41] Thus, by controlling the voltage, maximum heating temperature for these actuators was kept at 180°C, below the onset of these effects. The effect of elastomer layer thickness on the bending displacement for samples ranging from 0.2 to 2.5-mm thick is shown in Figure 1a. These samples were actuated with 2.5 cm

Figure 1. Electrothermal actuator (ETA) characterization graphs. (a) Displacement as a function of temperature for 0.2-mm, 0.5-mm, 1.0-mm, 1.5-mm, 2.0-mm, and 2.5-mm-thick ETAs. (b) Displacement versus temperature for ETA samples during cooling to room temperature. (c) Maximum displacement at 180°C for various clamping length of a 1.0-mm-thick sample. (d) Example of clamped length. (e) Heating time for ETAs of different volumes continuously supplied 8 V. (f) Cooling time for ETAs of different volumes at room temperature.

between the constraints, and the resulting center displacement was recorded. The resulting maximum deflection in the 1.0-mm sample was recorded as 2.3 mm from the starting position, which is a near 50% increase from the 0.5-mm-thick sample (1.5-mm maximum deflection), and near triple the amount of the thinnest 0.2-mm sample (0.8-mm maximum deflection). Less contrast was observed among the relatively thicker samples (1.5 mm, 2.0 mm, and 2.5 mm) where the peak displacements were recorded as 2.4 mm, 2.2 mm, and

2.1 mm, respectively. A positive relation between increases to initial thickness and thermal expansion producing greater maximum displacement is observed up to the 1.5-mm-thick sample. Increasing to the thickness beyond the 1.5-mm mark resulted in decreases to the actuation displacement indicating that the most favorable thickness to displacement ratio is found at 1.5-mm thickness for the chosen actuator length and width. The lower deflection for the thinner samples (0.2 mm and 0.5 mm) is a result of insufficient thermal expansion of

the thinner elastomer layers to produce the buckling behavior between the fixed constraints. The decreasing trend of peak displacement for the samples with thicknesses above 1.5 mm is a consequence of an excess of elastomer not contributing to the deformation. Figure 1b shows the cooling trend for the 0.5-mm, 1.0-mm, and 2.0-mm-thick samples. In terms of the shape recovery, a greater initial drop in displacement is observed in the 1.0-mm and 2.0-mm samples going from 180 to 170°C compared to the thinner sample.

The relationship between the dimensions of the ETA sample and the maximum deflection can be expressed through the equation of a beam in bending with both ends fixed under a uniform load:

$$\delta_{max} = F \cdot L^4 / (384 \cdot E \cdot I), \qquad 1$$

where δ_{max} is the maximum deflection at the center of the beam, F is the uniformly distributed load, L is the length of the beam, E is the modulus of elasticity, and I is the area moment of inertia. After inserting the area moment of inertia for a solid rectangular cross-section beam,

$$I_x = (w \cdot h^3)/12 \qquad 2$$

and simplifying the equation to the dimensional variables, the equation becomes:

$$\delta_{max} \propto L^4/(w \cdot h^3), \qquad 3$$

where w is the width and h is the height of the beam.[42] The term for height is equivalent to the combined thickness of the PDMS/CNT bilayer in this study. Based on Equation 3, it can be observed that maximum deflection is inversely proportional to the total thickness. An optimal thickness for the construction of ETA samples is in the range of 1.0–1.5 mm. Further decreases to thickness would affect the peak displacement and stability, whereas increases to the thickness beyond this range would not enhance the maximum deflection, but would raise the overall heating time due to the larger volume for the heat permeation.

The next observation was on the clamping distance, as shown in Figure 1c−d. The clamping length is denoted as the distance between the mechanically clamped points to constrain thermal expansion of the ETA. To accurately compare its effect, a 1.0-mm-thick sample was tested while shortening the clamped length for each trial. The series of clamped lengths tested ranged from 1.0 to 3.0 cm in intervals of 0.5 cm. Reducing the clamped length by 0.5 cm segments significantly reduced the maximum displacement below 2.5-cm clamping length. The largest decrease was between the 2.0 and 1.5-cm clamping length, where the maximum displacement drops from 1.7 to 0.8 mm. Increasing clamping length to 3 cm had a minimal effect on the maximum displacement, remaining in the range of 2.2 mm. In contrast to the thickness, Equation 3 expresses the relationship between maximum deflection and length to be directly proportional and to a higher power than the thickness, which explains the more pronounced effect. The marginal decrease in maximum displacement at 3.0-cm

clamping length is due to the practical constraint with the sample thickness not producing sufficient thermal expansion over the entire actuator length.

Figure 1e−f shows the trend of overall heating and cooling time for a standard actuation cycle of ETAs of the same width and length, but different thicknesses. The heating time was recorded as the actuation time of the ETA required to reach 180°C while being supplied 8 V, whereas the cooling time was the duration of time taken to air-cool to room temperature. The heating time approximately doubles for each step increase in volume between 0.6 and 4.5 cm³ and doubled from 4.5 to 7.5 cm³. Proportional to the increase in volume, a greater input power is required to maintain the same heating time. Similarly, the observed cooling time increases substantially as the volume increases. The cooling time doubles from 0.6 to 3.0 cm³, and once again from 3.0 to 7.5 cm³. In the absence of active cooling, the time to reset to the initial thermal state is considerably longer than the actuation time. The series of characterization tests reveal the geometric dependence of clamped bending actuation on length and thickness, as well as the heating time and cooling trends of ETAs.

Morphology of ETAs

In the previous section, the ETAs analyzed were fabricated through solvent casting the CNT conductive layer and curing the PDMS elastomer layer on top. When examined using scanning electron microscopy (SEM [**Figure 2**a−b]), the solvent casted samples had large variations in CNT layer thickness. Sections were observed where the thickness is measured to be nearly twice as much as adjacent sections, ranging from 18.9 to 34.5 μm in the observed area. The fluctuations in thickness can be attributed to the solvent casting fabrication process causing randomness in CNT settlement during evaporation and losses during removal from the casting container. This nonuniformity suggests some regions within the actuator will have greater electrical resistance than others, creating localized heating zones and contributing to nonsymmetrical thermal expansion.

To diminish this effect, it is theorized that increasing the uniformity in thickness of the conductive layer will improve the uniformity in heating distribution, bending consistency, and deformation. A vacuum filtration method was used to recover a CNT layer on a solvent permeable membrane. After curing a layer of PDMS on top, the cross section was inspected, as shown in Figure 2c. The vacuum-filtered ETA had considerably lower variation in layer thickness, within 4 μm. In addition to the uniformity in thickness, multiple actuators could be created using the same CNT buckypaper, leading to easily replicable actuators with consistent conductive layer properties.

Another approach to increase heating distribution and efficiency was attempted by fabricating trilayered ETAs. This method completely encases the CNT layer within the elastomer, which greatly reduces the heat loss ordinarily present in
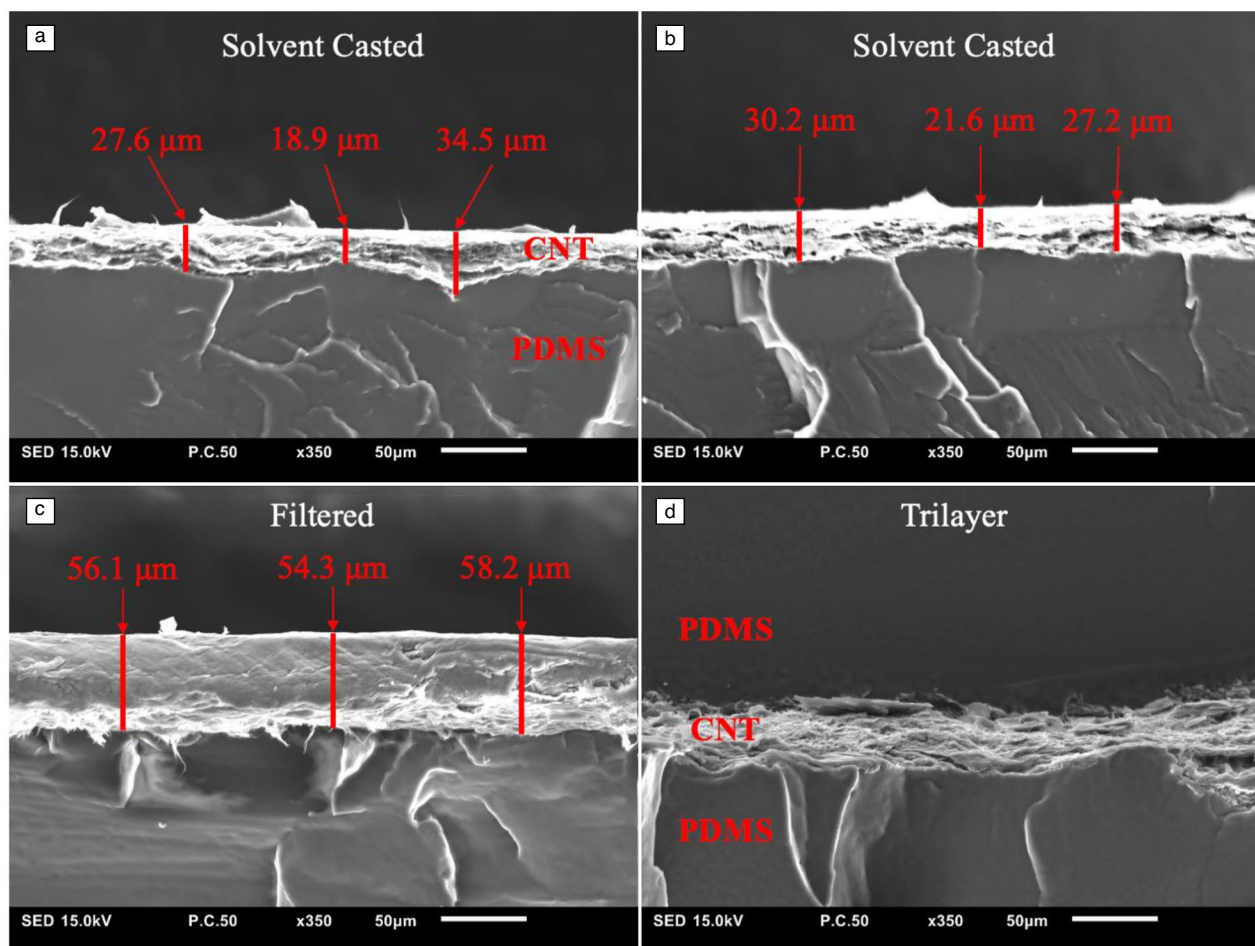
Figure 2. Scanning electron microscope images showing the cross section and measured carbon nanotube conductive layer thickness of (a) and (b) two solvent casted, (c) filtered, and (d) trilayer electrothermal actuators.

the bilayer actuator through the uncovered areas. The upper layer of PDMS in this design was fabricated to be twice the thickness compared to the bottom layer. This causes the bending deformation to favor curling toward the thinner layer because the thermal expansion is greater in the thicker side. Figure 2d shows the interaction region of the CNT layer from both sides with PDMS.

Actuation of alternative ETAs

By utilizing the vacuum-filtration fabrication processes, various improved electrothermal actuator configurations were constructed. To compare the behavior of these configurations, the actuation of solvent casted and filtered bilayer, and a solvent casted trilayer ETA (all with an overall thickness of 1 mm) were compared as shown in **Figure 3**. In the case of the solvent casted bilayer configuration, the maximum deflection upon initially reaching 180°C was 2.3 mm. The heating cycle time was 60 s, and the average input power was 5.65 ± 0.32 W in the three attempted tests. In comparison, the ETA created by

filtration of the conductive layer was observed to have a peak displacement of 2.0 mm from the initial position. In the three trials of this sample, the heating took approximately 50 s and the power required for this was 2.70 ± 0.15 W.

Although producing a lesser magnitude of bending actuation, the filtration-produced ETA could successfully reach the desired maximum temperature of 180°C faster and with substantially reduced input power (50% of the solvent casted ETA). The filtration method produces a more densely packed CNT layer, which is responsible for the faster heating speed and lower power input. However, the difference in displacement results can be attributed to the greater thickness of the conductive layer in the filtration method restricting the contraction and bending of the elastomer. An additional benefit to using the filtration method was the consistency in the fabrication process. For applications where the shape morphing is desired in specific locations and in certain shapes, such as arrays, a high degree of reproducibility and precision is necessary. The filtration-produced CNT buckypaper could be
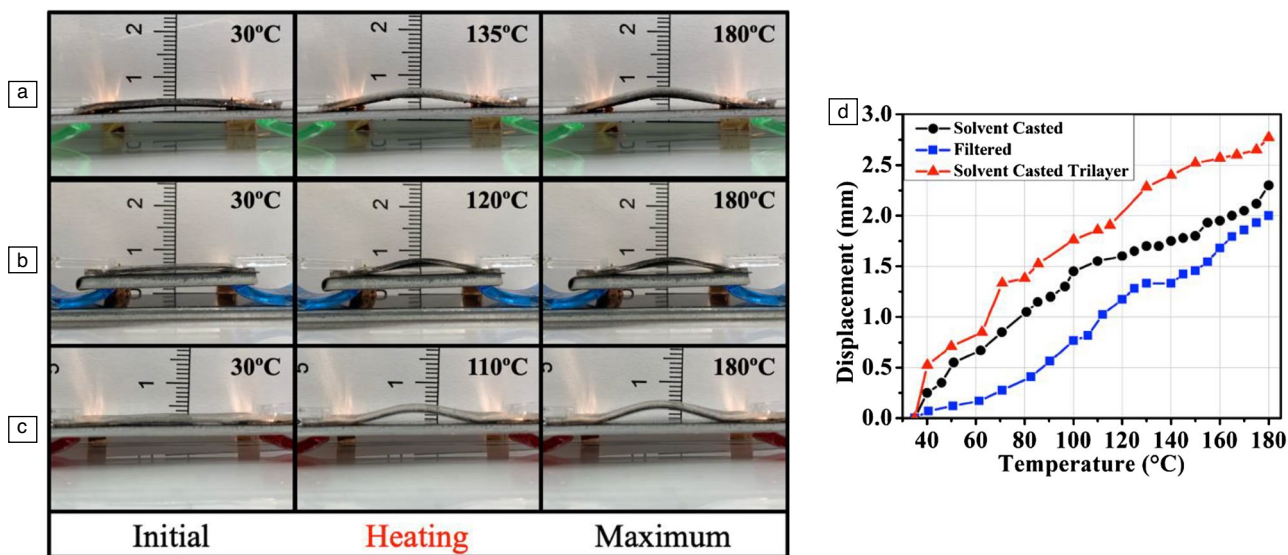
Figure 3. Actuation of (a) solvent casted bilayer, (b) filtered bilayer, (c) solvent casted trilayer. All samples have a thickness of 1 mm and clamped length of 2.5 cm. **(d)** Displacement versus temperature for the three samples.

reduced to the desired shape and size through precise incisions, whereas solvent casting requires an enclosed area for solvent evaporation and will not necessarily result in reproducible samples for the determination of input power to heating. The actuation characterizations reveal that the assembly of a bilayer ETA can be simplified through the use of filtration-produced buckypaper.

The most notable improvement in the maximum deflection (2.8 mm) was displayed in the trilayer configuration. Compared to the solvent casted bilayer, the increase in deflection is caused by the lesser expansion of the bottom layer of PDMS drawing the upper layers downward and in tension. As the thermal absorption is observed to be the main contributor to the heating speed, the increases to the actuation response time results from the increased coverage of the CNT heating layer.

ETA application as a soft and flexible surface morphing array

To demonstrate the feasibility of utilizing ETAs, a soft and flexible surface morphing sheet was created using filtered CNT buckypaper as presented in **Figure 4**a. The size and arrangement of activatable segments are adaptable during fabrication by altering the specific location of buckypaper placement. The actuator array is shape conformable, which enables it to be attached on flat and rounded surfaces—in this case on the inner surface of an air duct, as shown in Figure 4b, inspired by S-shaped ducts employed on air vehicles with embedded engines.[43] For this specific application, the shape-morphing feature of the ETA array provides for the gradual narrowing of the duct inlet, which could be employed to control the air flow

rate and pressure. Figure 4c shows the integration of the actuator electrodes to supply power for the heating. This actuator array sheet is attached to the substrate using adhesives around where the surface morphing is desired. The produced PDMS/CNT actuator array sheet consists of multiple ETA segments where locations with the CNT layers are capable of bending actuation in both an individual and simultaneous fashion (Figure 4d). The elastomer and CNT layers are strongly bonded and flexible enough such that application is not restricted to flat surfaces, as shown in this demonstration. Minimal differences in maximum displacement were observed between the different ETA orientations along the inner surface (i.e., between actuators on the top, bottom, and side surfaces) as the buckling stresses that produce the bending deformation are expected to be much greater than any effects due to gravity.

It was noted that to produce the well-defined and independent hill shapes as shown, the activatable CNT loaded sections were separated by 10-mm nonconductive sections. The adhesive is applied directly along the center of the nonconductive sections, acting as constraints for the conductive segments. This resulted in an additional clamped spacing of 1 cm when considering the width and unclamped spacing between adjacent segments. With these dimensions, each segment was able to activate without hindering the adjacent segments. The displayed model revealed that the designed actuator array can produce surface features on the applied area to alter the overall geometry. Characterization of the various design configurations furthered the suitability of employing ETAs as surface morphing soft actuators, and the inherent flexibility allows it to be applied to a variety of substrates.
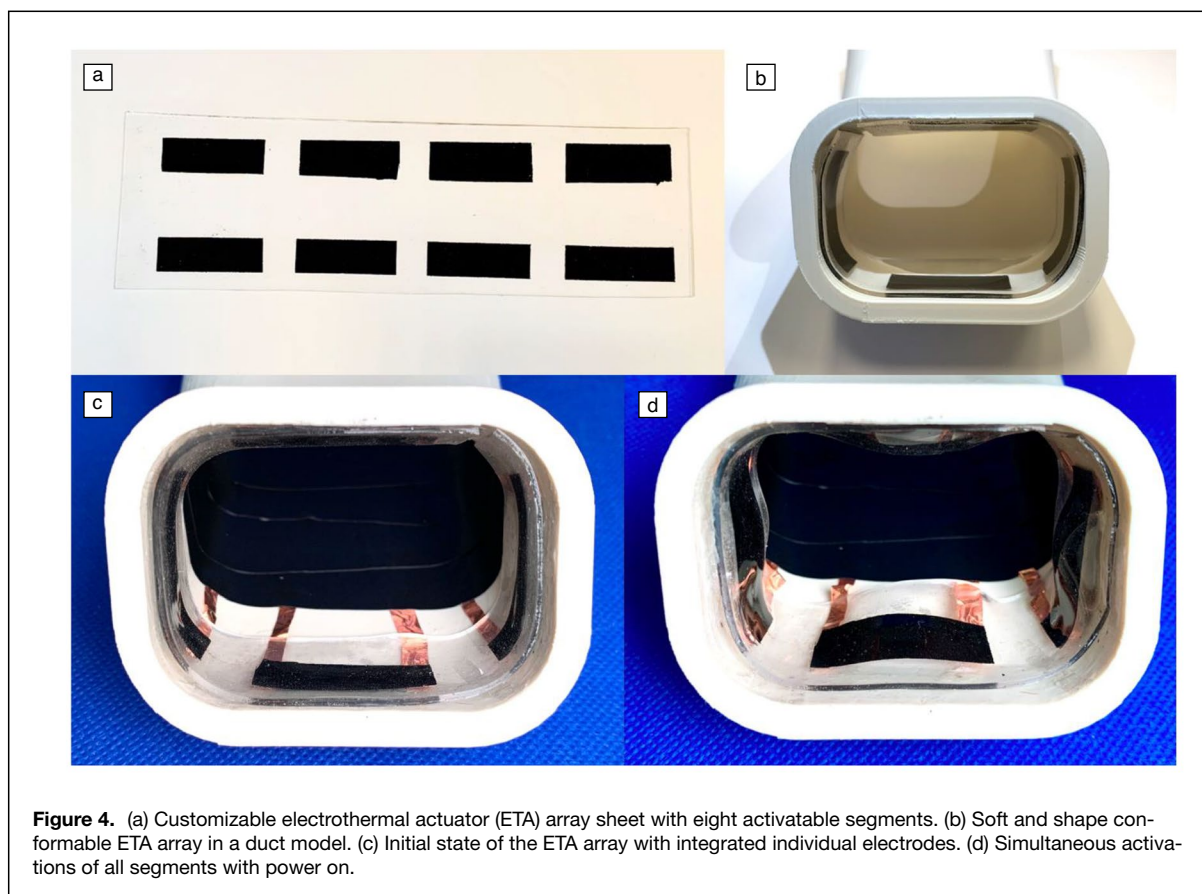
Figure 4. (a) Customizable electrothermal actuator (ETA) array sheet with eight activatable segments. (b) Soft and shape conformable ETA array in a duct model. (c) Initial state of the ETA array with integrated individual electrodes. (d) Simultaneous activations of all segments with power on.

Conclusion

This article presented the design characteristics and fabrication of electrothermal actuators as soft and flexible surface morphing actuators capable of deforming into specifically designed local features. These ETAs were created by either solvent casting or vacuum filtering dispersed SWCNTs and curing a PDMS elastomer layer on top to generate both a conductive and flexible bilayer with distinct thermal expansion rates. The design parameters, such as overall dimensions and actuation time, were characterized through fixed-beam bending configuration tests. The tests revealed that increasing the distance between the fixed supports significantly increases bending deflection, from 1.7 to 2.3 mm when increased from 2 to 2.5 cm clamped length. SEM cross-sectional views showed the smaller thickness variations in the CNT conductive layer when using the filtration method compared to the solvent casting method. By utilizing the knowledge of all the design parameters, the newly developed trilayer ETA was actuated and was found to have 22% increased displacement. In addition, an array of ETAs was fabricated as single continuous sheet, where each segment was individually and simultaneously activated to create complex surface features. To demonstrate its potential for aerospace application, a model air duct was fabricated with an integrated ETA array attachment to showcase the surface morphing ability. The shape and location of the actuatable regimes were shown to be adjustable in

the manufacturing phase to allow specifically designed ETA arrays for potential aerodynamic applications in drag control. Beyond the described examples, the presented work on ETAs, with their fabrication methods and design parameters, suggest potential applications for these composites in the areas of soft robotic actuators and morphing surfaces.

Materials and methods

Single-walled carbon nanotubes (SWCNTs, TUBALL) were obtained from OCSiAl. The technical specifications for the SWCNT material were stated as 76 wt% SWCNT content, ≤ 15 wt% metal impurities, and a 1.6 ± 0.4 nm outer diameter range. The silicone elastomer chosen was a poly(dimethylsiloxane) (PDMS, Sylgard 184, Dow Inc.). This was provided as a two-part kit, base polymer and curing agent, with a recommended 10:1 curing ratio. Stretchable conductive paint, silver conductor (PE873, DuPont) was used as electrical contacts.

Fabrication and characterization of PDMS/CNT electrothermal actuator

Figure 5a provides a schematic representation of the fabrication process of the PDMS/CNT ETA. SWCNTs were dispersed in acetone solution at 0.83 mg/mL by ultrasonication. The ultrasonication settings were 50% amplitude, 4 s
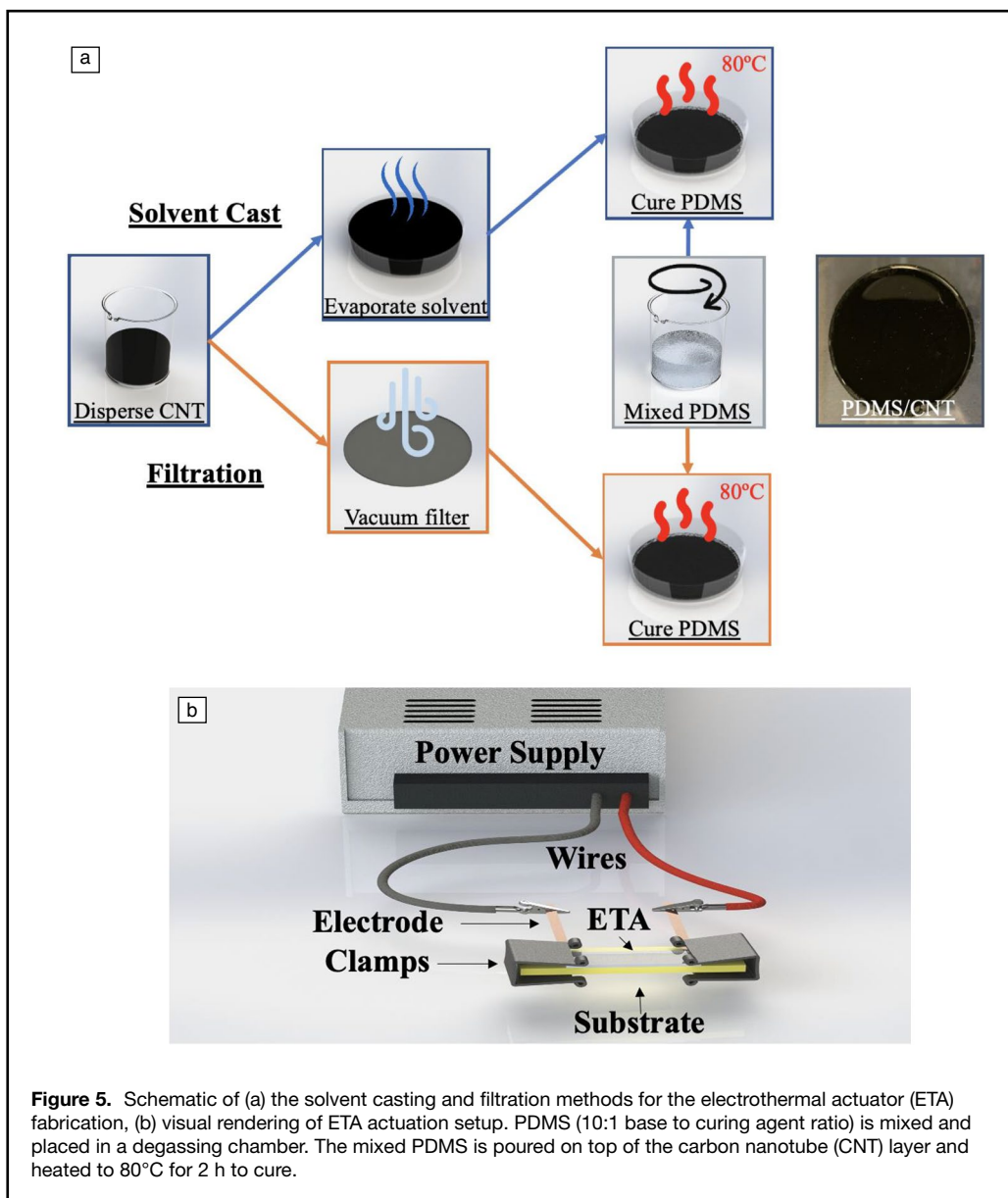
Figure 5. Schematic of (a) the solvent casting and filtration methods for the electrothermal actuator (ETA) fabrication, (b) visual rendering of ETA actuation setup. PDMS (10:1 base to curing agent ratio) is mixed and placed in a degassing chamber. The mixed PDMS is poured on top of the carbon nanotube (CNT) layer and heated to 80°C for 2 h to cure.

on a solid nonconductive substrate and mechanically clamped on both ends with the copper electrodes extending out. The electrodes were connected to a DC power supply by electrical wires that would initiate the Joule heating process. The current passing through the conductive layer of the ETA would initiate Joule heating, causing thermal expansion of the elastomer layer. The increase in temperature is captured by a thermal camera and the difference in bending height from the initial to the activated state of the sample is video recorded.

To observe the differences in performance, the SWCNT conductive layer was also fabricated using a filtration method. SWCNTs dispersed in acetone using the same ultrasonication conditions were filtered under vacuum using a filter membrane. The filter membrane holding the dispersed CNTs was covered, placed under weights to prevent shrinkage, and dried in an oven at 80°C. Once the CNT buckypaper was completely dried, it was cut and

on, 2 s off pulse duration, for a total of 65 min time while also being magnetically stirred. The sonicated SWCNT/acetone solution was poured into a petri dish and left at room temperature until the solvent completely evaporated. In a separate container, PDMS was hand-mixed at a 10:1 base to curing agent ratio and placed in a degassing chamber to remove the trapped air bubbles. Subsequently, a controlled amount of the mixed PDMS corresponding to the desired elastomer thickness was poured on top of the CNT layer and heated to 80°C for 2 h to cure. The cured PDMS/CNT sample was removed from the dish and cut into rectangular pieces of 1 × 3 cm. Thin copper foil sheets were attached as electrodes on both ends of the actuator using silver paste to ensure electrical connection.

The ETA samples were arranged as displayed in Figure 5b to observe actuation. The ETA sample was placed

placed onto a petri dish and mixed PDMS was poured over top. Trilayer ETAs were created by partially curing a PDMS layer onto the petri dish prior to beginning the original fabrication process. This bottom layer of PDMS used half of the amount of the expected upper layer to provide directional bias when heating.

Several properties that influence the actuation behavior of the ETA were investigated. The ultimate tensile strength and elastic modulus were characterized using coupon geometries drawn from ASTM D638 Type IV standards using an Instron (5848 MicroTester, Instron). A Keithley 2400 source meter and a four-point probe were used to measure the resistance of the conductive layer. Scanning electron microscopy (SEM, JSM-IT100, JOEL Inc.) was utilized on the cryo-fractured cross section to observe the variation in the conductive layer thickness from the different fabrication processes.

Acknowledgments

Data availability

The data sets generated and analyzed during the current study are available from the corresponding author on reasonable request.

Conflict of interest

The authors declare no conflict of interests.

References

1. A. Potekhina, C. Wang, *Actuators* **8**(4), 69 (2019). https://doi.org/10.3390/act8040069
2. Y. Hao, S. Zhang, B. Fang, F. Sun, H. Liu, H. Li, *Chinese J. Mech. Eng.* **35**, 37 (2022). https://doi.org/10.1186/s10033-022-00707-2
3. P. Won, K.K. Kim, H. Kim, J.J. Park, I. Ha, J. Shin, J. Jung, H. Cho, J. Kwon, H. Lee, S.H. Ko, *Adv. Mater.* **33**(19), 2002397 (2021)
4. M. Mrinalini, S. Prasanthkumar, *ChemPlusChem* **84**(8), 1103 (2019)
5. H.S. Tzou, H.J. Lee, S.M. Arnold, *Mech. Adv. Mater. Struct.* **11**(4–5), 367 (2004)
6. S. Kim, C. Laschi, B. Trimmer, *Trends Biotechnol.* **31**(5), 287 (2013)
7. R. Yin, B. Yang, X. Ding, S. Liu, W. Zeng, J. Li, S. Yang, X. Tao, *Adv. Mater. Technol.* **5**(8), 2000441 (2020). https://doi.org/10.1002/admt.202000341
8. Z. Zhang, Y. Li, X. Yu, X. Li, H. Wu, H. Wu, S. Jiang, G. Chai, *Thin-Walled Struct.* **142**, 74 (2019)
9. A.C. Henry, G. Molinari, J.R. Rivas-Padilla, A.F. Arrieta, *AIAA J.* **57**(6), 2384 (2019)
10. S. Shian, K. Bertoldi, D.R. Clarke, *Adv. Mater.* **27**(43), 6814 (2015)
11. S.K. Mitchell, X. Wang, E. Acome, T. Martin, K. Ly, N. Kellaris, V.G. Venkata, C. Keplinger, *Adv. Sci.* **6**(14), 1900178 (2019). https://doi.org/10.1002/advs.201900178
12. M.E.M. Salem, Q. Wang, *Eng. Res. Express* **4**(1), 015001 (2022)
13. O. Kim, S.J. Kim, M.J. Park, *Chem. Commun.* **54**(39), 4895 (2018)
14. D. Mao, F. Hu, Z. Yi, Kenry, S. Xu, S. Yan, Z. Luo, W. Wu, Z. Wang, D. Kong, X. Liu, B. Liu, *Sci. Adv.* **6**(26), eabb2712 (2020)
15. M. Bashir, P. Rajendran, *J. Intell. Mater. Syst. Struct.* **29**(19), 3681 (2018)
16. Y. Bar-Cohen, I.A. Anderson, *Mech. Soft Mater.* **1**, 5 (2019). https://doi.org/10.1007/s42558-019-0005-1
17. L. Chen, M. Weng, Z. Zhou, Y. Zhou, L. Zhang, J. Li, Z. Huang, W. Zhang, C. Liu, S. Fan, *ACS Nano* **9**(12), 12189 (2015)
18. Q. Li, C. Liu, Y.H. Lin, L. Liu, K. Jiang, S. Fan, *ACS Nano* **9**(1), 409 (2015)
19. S. Yao, J. Cui, Z. Cui, Y. Zhu, *Nanoscale* **9**(11), 3797 (2017)
20. P.J. Cottinet, C. Souders, S.Y. Tsai, R. Liang, B. Wang, C. Zhang, *Phys. Lett. A* **376**(12–13), 1132 (2012)
21. I.A. Rousseau, *Polym. Eng. Sci.* **48**(11), 2075 (2008)
22. Y. Yang, Y. Wu, C. Li, X. Yang, W. Chen, *Adv. Intell. Syst.* **2**(1), 1900077 (2020)
23. Q. Li, C. Liu, S. Fan, *Nanotechnology* **29**(17), 175503 (2018)
24. G. Tibi, E. Sachyani Keneth, M. Layani, S. Magdassi, A. Degani, *Soft Robot.* **7**(5), 649 (2020)
25. Y. Tian, Y. Li, Q. Wang, H. Tian, X. Geng, Y. Zhi, Y. Wei, Y. Yang, T. Ren, "A Soft Electrothermal Actuator with Large Deformation and High Periodic Deformation Speed," *2020 21st International Conference on Electronic Packaging Technology (ICEPT 2020)* (IEEE, Guangzhou, August 12–15, 2020), pp. 1–4
26. Z. Zhou, Q. Li, L. Chen, C. Liu, S. Fan, *J. Mater. Chem. B* **4**(7), 1228 (2016)
27. Z. Li, Z. Liang, *Sci. Rep.* **7**, 42423 (2017). https://doi.org/10.1038/srep42423
28. Y. Jang, S.M. Kim, G.M. Spinks, S.J. Kim, *Adv. Mater.* **32**(5), 1902670 (2020)
29. L. Xue, W. Wang, Y. Guo, G. Liu, P. Wan, *Sens. Actuators B Chem.* **244**, 47 (2017)
30. S.A. Meguid, G.J. Weng, *Micromechanics and Nanomechanics of Composite Solids* (Springer, New York, 2017)
31. J.N. Coleman, U. Khan, W.J. Blau, Y.K. Gun'ko, *Carbon* **44**(9), 1624 (2006)
32. R.I. Rubel, M.H. Ali, M.A. Jafor, M.M. Alam, *AIMS Mater. Sci.* **6**(5), 756 (2019)
33. B. Ribeiro, J.A.R. Corredor, L. Ardila, L.F.P. Santos, M.L. Costa, M.C. Rezende, E.C. Botelho, *J. Appl. Polym. Sci.* **137**(5), 48330 (2020)
34. J. Ahn, Y. Jeong, Z.-J. Zhao, S. Hwang, K. Kim, J. Ko, S. Jeon, J. Park, H. Kang, J.-H. Jeong, I. Park, *Adv. Mater. Technol.* **5**, 1900997 (2020). https://doi.org/10.1002/admt.201900997
35. Y. Martinez-Rubi, B. Ashrafi, M.B. Jakubinek, S. Zou, K. Laqua, M. Barnes, B. Simard, *ACS Appl. Mater. Interfaces* **9**(36), 30840 (2017)
36. W. Sang, L. Zhao, R. Tang, Y. Wu, C. Zhu, J. Liu, *Macromol. Mater. Eng.* **302**(12), 1700239 (2017)
37. Y. Cao, J. Dong, *Procedia Manuf.* **48**, 43 (2020)
38. Q. Fan, J. Miao, M. Tian, H. Zhao, S. Zhu, X. Liu, Y. Ma, L. Qu, *Sens. Actuators A Phys.* **315**, 112352 (2020)
39. Y.-C. Sun, B.D. Leaker, J.E. Lee, R. Nam, H.E. Naguib, *Sci. Rep.* **9**(1), 11445 (2019)
40. E. Hajiesmaili, D.R. Clarke, *Nat. Commun.* **10**(1), 10 (2019)
41. M. Liu, J. Sun, Q. Chen, *Sens. Actuators A Phys.* **151**(1), 42 (2009)
42. J.M. Gere, *Mechanics of Materials*, 6th edn. (Thomson-Engineering, Belmont, 2006)
43. A. Asghar, S. Sidhu, W.D.E. Allan, G. Ingram, T.M. Hickling, R. Stowe, "Investigation of a Passive Flow Control Device in an S-Duct Inlet of a Propulsion System with High Subsonic Flow," in *Proceedings of the ASME Turbo Expo 2018: Turbomachinery Technical Conference and Exposition. Volume 1: Aircraft Engine; Fans and Blowers; Marine* (Oslo, 2018), pp. 1–18 □